Journal of Materials Research and Technology 35 (2025) 152–163

Contents lists available at ScienceDirect

Journal of Materials Research and Technology

journal homepage: www.elsevier.com/locate/jmrt

An all-weather anti/de-icing coating combining superhydrophobic surfaces with photothermal and electrothermal functions

Xiuzhang Qin [a,b,1], Jiaxu Wang [a,1], Yu Dai [a,1], Jin Xu [a,c,1], Jingfu Jin [a,b], Tingkun Chen [a,*], Mingqing Wang [d]

[a] College of Biological and Agricultural Engineering, Key Laboratory of Bionic Engineering (Ministry of Education), Jilin University, Changchun, 130022, PR China
[b] Sichuan Key Technology Engineering Research Center for All-electric Navigable Aircraft, Sichuan, Guanghan, 618307, PR China
[c] School of Modern Industry, Jilin Jianzhu University, Changchun, 130118, PR China
[d] Institute for Materials Discovery, University College London, London, WC1E 7JE, United Kingdom

ARTICLE INFO

Handling editor: Prof. M Meyers

Keywords:
Ice adhesion
Photothermal
Electrical
Superhydrophobic
All-weather anti/de-icing
Freezing interface strain

ABSTRACT

To reduce the hazard of ice adhesion, a superhydrophobic coating with a contact angle of 150.4°, a sliding angle of 2°, and high light absorption performance was applied to the aluminum surface in the present study. The phase transition time of water on the superhydrophobic photothermal coating surface was delayed by 82.70 s compared to the freezing time of water on the aluminum alloy surface at −5 °C. Under the same light intensity, the melting time of the accumulated ice on the GPSC surface was 445.60 s; however, the melting of the covered ice on the aluminum alloy surface did not occur. The energy consumption required to melt the accreted ice on the GPSC surface using electric heat was 55.63% lower than that for melting ice on the aluminum alloy surface. The contact angle of the GPSC surface was measured at 143.6° after being impacted by 4 kg of quartz sand. Coating the material surface with GPSC could enhance the passive anti-icing performance of the material. When combined with a low-power electric heating method to melt the ice on the surface, this would create an all-weather anti/de-icing strategy that merges both active and passive approaches to remove ice from component surfaces. Additionally, the interface strain could change suddenly during the freezing process of water on different material surfaces at varying temperatures. This research could support ice monitoring techniques in the engineering field as well as assist in determining the optimal starting time for anti/de-icing methods.

1. Introduction

Ice adhesion occurs when moisture in the environment adheres to cold surfaces, undergoes a phase change to freeze into ice, and forms an adhesion strength between the material, which is not easy to remove from the material surface. Although it can be seen that ice adhesion is a common natural phenomenon, it has posed serious hazards to the engineering field [1]. As wind turbines are often installed in high altitude or humidity areas, ice or snow adheres to the surfaces of turbine blades, gearboxes, anemometers, and other components [2–5]. It alters the shape and centroid of the blade, leading to abnormal vibrations of the wind turbine, voltage instability, reduction in operation safety, etc. [6–8]. Statistically, the loss of turbine capacity due to ice adhesion is approximately 50% of the annual grid-connected generation [9,10]. Additionally, ice adhesion can increase the load on components and affect operation safety, which has a particularly significant impact on the power transmission field. For example, during the freezing disaster in southern China in 2008, the transmission line and tower collapsed due to the increased load caused by ice adhesion [11–14]. The freezing disaster has caused widespread paralysis of the power grid in the south of China, with direct economic losses exceeding 150 billion RMB [15,16]. Meanwhile, ice adhesion can also change material surface properties, such as thermal conductivity and light transmission [17,18]. As one of the key components of cold chain logistics, evaporators, condensers, etc., are prone to accumulate a large amount of frost and ice layers on their surfaces, which seriously affects the equipment operation efficiency and reduces the storage quality of agricultural and sideline products [19–21]. Meanwhile, the influence of ice adhesion on

* Corresponding author. College of Biological and Agricultural Engineering, Key Laboratory of Bionic Engineering (Ministry of Education), Jilin University, Changchun, 130022, PR China.
E-mail address: chentk@jlu.edu.cn (T. Chen).
[1] X.Q., J.W., Y. D. and J.X. contributed equally to this work.

https://doi.org/10.1016/j.jmrt.2025.01.038
Received 1 November 2024; Received in revised form 25 December 2024; Accepted 6 January 2025
Available online 7 January 2025

high-speed rail operation performance has become increasingly evident as the global high-speed rail operation mileage increases. If ice or snow adheres to the surfaces of the bogie, suspension, and other components of the high-speed rail chassis, it will affect the steering freedom of high-speed rail and passenger comfort [22–26]. Additionally, ice adhesion can also have a serious influence on engineering fields, such as aircraft, ships, communication, photovoltaics, and construction [27–34].

To mitigate the harm of ice adhesion and develop anti/de-icing methods, researchers have begun to explore the ice adhesion mechanism, such as the mechanical anchor effect, liquid-like layer, chemical bonding, electrostatic interaction, and so on [35–38]. Meanwhile, the influence of temperature, wettability, water composition, and other factors on ice adhesion have been studied [39–44]. For example, the ice adhesion strength gradually increases and tends to be stable with decreasing temperature [42–44]; adding sodium chloride to water can delay the freezing time as well as reduce the ice adhesion strength [45,46]. Based on the mechanism of ice adhesion and the influence factors on ice adhesion strength, many kinds of anti/de-icing methods have been developed to remove the accumulated ice, which can be divided into active and passive anti/de-icing methods [47–49].

At present, active anti/de-icing methods, such as mechanical methods using external force, thermal solutions to improve surface temperature to postpone the phase time of water and melt the accumulated ice, and chemical methods by spraying anti/de-icing to delay freezing, have been widely used in engineering [50,51]. Although active anti/de-icing methods have been widely used, there are many drawbacks such as complex systems, high energy consumption and cost, environmental pollution, etc. [52–55] For example, when the chemical anti/de-icing method is used to remove the accreted ice, a large amount of anti/de-icing will be required, and the used anti/de-icing agent will result in soil hardening, water resource pollution, and so on [56,57]. However, with the discovery of the lotus effect, it is possible to reduce the attached amount of water and decrease the contact area between water and material by enhancing the wettability of the material surface to exhibit superhydrophobicity. So, the superhydrophobic coating is regarded as the passive anti/de-icing method and is considered one of the promising anti/de-icing methods in the future due to its remarkable properties. Many engineering fields have begun to explore the application of superhydrophobic surfaces in their respective fields, such as liquid manipulation [58], crude oil pollution [59], thermal camouflage and infrared anti-counterfeiting [60], and anti/de-icing [61]. However, some results have demonstrated that the superhydrophobic anti/de-icing coating has shortcomings, such as durability, mechanical stability, etc. [62–69] For example, Geng and He have repeatedly the connection strength between the superhydrophobic coating and the substrate using the tape and found that the wettability of the coating gradually decreased [68]. Kulinich et al. found that after freeze-thaw cycles, the anti/de-icing effect of the superhydrophobic surface prepared during the test would be reduced owing to the coating surface microstructure damage [69]. With the continuous development of material fabrication processes, many methods have been developed to prepare superhydrophobic surfaces, such as brushing [70], scraping [70], dipping [70–73], spraying [71,74–78], liquid-phase deposition [79], self-assembly [79], chemical deposition [71], sol-gel method [80], scraping [81], etc. Therefore, the spraying method which is simple to prepare and easy to apply in engineering, is used to prepare the functional coating on the substrate surface.

It can be seen that both active and passive anti/de-icing methods have their advantages respectively. Therefore, a combined passive and active anti/de-icing method can be developed by utilizing the advantages of active and passive anti/de-icing methods. As an inexhaustible renewable energy source, solar energy has been widely used and promoted, such as photovoltaic power generation, photovoltaic heat collection, agriculture, and so on [82,83]. Therefore, solar energy can be utilized to raise the material surface temperature, making the attached water less likely to freeze and adhere to the material surface in low-temperature environments. During the present study, a superhydrophobic coating with strong light adsorption was coated on the material surface, and the increased surface temperature after absorbing solar energy could delay the freezing time or melt the accumulated ice. Meanwhile, combined with the commonly used electrothermal method in active anti/de-icing techniques, the accumulated ice could be melted by heating when there is weak/no sunshine. Hence, the purpose of all-weather anti/de-icing coating would be achieved. Additionally, the interface strain between water and substrate was collected owing to the variation in contact diameter formed between water and substrate during the phase transition of attached water, and this could lay a theoretical foundation for proposing a new anti/de-icing strategy in engineering.

2. Materials and methods

2.1. Anti/de-icing model

Fig. 1 shows the all-weather anti-deicing model proposed in the present study. The functional coating with photo-thermal and superhydrophobic properties is sprayed on the material surface, and a low-power electrothermal film is pasted or fixed underneath the material.

It is well known that water is not easily adhered to superhydrophobic surfaces, and the coating with the photothermal function can absorb the solar energy to raise the surface temperature to delay the phase change time of the attached water to ice or melt the accumulated ice at the interface to decrease the ice adhesion strength. This will contribute to reducing the difficulty of removing the accreted ice. When sunlight is not available, the specimen is heated using a low-power electrothermal film fixed to the material bottom to melt the covered ice. The electrothermal film can be powered by the electricity generated by solar photovoltaic panels or other power sources.

Meanwhile, it is necessary to determine the working time of the electrothermal film based on the state of the attached water to remove the accumulated ice. It is well known that the volume of water increases before and after freezing, while other materials undergo shrinkage at low temperatures. So, the freezing interface strain generated from the freezing process will be also discussed during the present study. A method that determines the starting time of active anti/de-icing methods based on the change law of the freezing interface strain may be proposed.

2.2. Materials

During the present study, the aluminum alloy was purchased from Harbin Dongbeilong Metal Co., Ltd. as the substrate. The size of the sample was 20 mm × 20 mm × 1 mm (L × W × H). The chemical composition of aluminum alloy used as the substrate in the experiment is Cu (0.15–0.40%), Mn (0.15%), Mg (0.80–1.20%), Zn (0.25%), Cr (0.04–0.35%), Ti (0.15–0.40%), Si (0.40–0.80%), Fe (less than 0.7%), and the remaining part is Al. The graphene purchased from Shenzhen Hongdachang Science and Technology Co., Ltd. was utilized to improve the surface absorption performance. SiO_2 powder was purchased from Jinan Mcc New Materials Co., Ltd. Epoxy resin, tetrahydrofuran, FAS-17, xylene, and deionized water were purchased from Liaoning Quanrui Reagent Co., Ltd.

2.3. Fabrication process of surfaces

SiO_2 particles with hydrophobic property is obtained by adding FAS-17 to a magnetically stirred SiO_2 dispersion in xylene, followed by magnetic stirring, centrifugation, and drying. 1.6 g of epoxy resin was added to 30 ml of tetrahydrofuran and stirred for 30 min. Subsequently, 0.6 g of modified SiO_2 powder was added to the mixed solution. After continued stirring for 15 min, 0.1 g of graphene powder was added. The

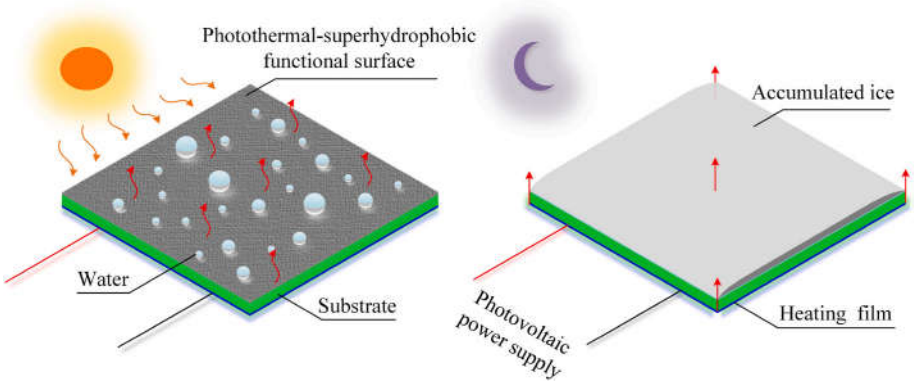

Fig. 1. All-weather anti/de-icing model.

mixed solution which was stirred for 10 min was sprayed on the aluminum alloy surface. The specimens with photothermal and superhydrophobic properties were obtained by drying at 90° ambient for 50 min. The superhydrophobic coating with light absorption property prepared during the present study was named GPSC.

2.4. Characterization

The contact angle of 20 μL of deionized water on the GPSC surface as well as the sliding angle were measured by OCA 20. The material composition of GPSC was analyzed by energy dispersive spectroscopy (X-Max50, Oxford Instruments Co., Ltd, UK). The coating surface was analyzed for micromorphology (Sigma 300, Zeiss Co., Ltd, Japan) and

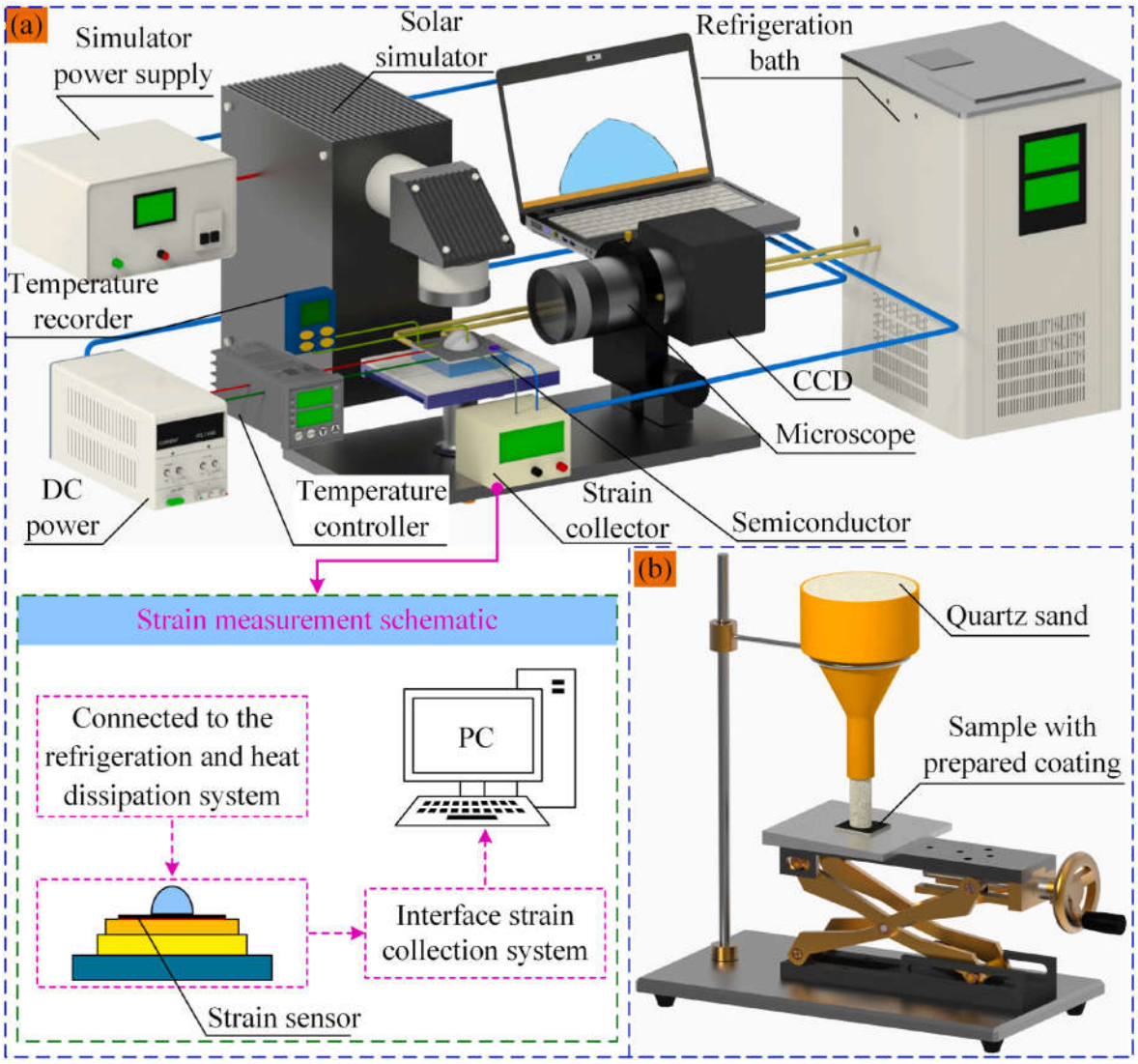

Fig. 2. Schematic diagram of the test device. (a) Multi-functional test apparatus; (b) Quicksand abrasion-resistant device.

the surface roughness of the coating was analyzed by OLS 3000 (Olympus Co., Ltd, Japan). A solar simulator was used to simulate sunlight irradiation to melt the accumulated ice on GPSC, and the light-absorbing properties of aluminum and GPSC were tested by UV/Vis/NIR spectrometer (UV-3600i Plus, Shimadzu Co., Ltd, Japan). Meanwhile, the infrared spectrum of the coating was measured using the Spectrum 3 (PerkinElmer Co., Ltd, US). A high-speed video camera (Phantom 9.1, Vision Research, Inc.) was utilized to record the bouncing process of droplets falling on GPSC. In the test, the mechanical stability of the GPSC was tested by quartz sand impacting the surface.

2.5. Experimental methods

2.5.1. Test device

Fig. 2 shows the self-built device used in the experiment. The multifunctional apparatus shown in Fig. 2 a could be used to observe the freezing process of water adhering to the cold surface as well as to collect the freezing interface strain. The device consists of a refrigeration system, a temperature control system, an icing observation system, a strain acquisition system, and other components that synchronize the observation of the freezing process and the acquisition of interface strain.

A thermoelectric device shown in Fig. 2 a is used to cool the cold surface as well as the attached water, and the refrigeration bath is utilized to dissipate heat generated from the semiconductor. A K-type thermocouple with an accuracy of ±0.01 °C is adopted to collect the internal temperature of the attached water. The refrigeration system and temperature control system in the device shown in Fig. 2 a can be used for solar simulation to melt the accreted ice.

The apparatus for the mechanical stability of GPSC was shown in Fig. 2 b. During the test, quartz sand (purchased from Hongdingxing Quartz Sand Factory, Guangxi) with a diameter of 0.5 mm–1.0 mm was utilized to impact the GPSC surface by falling from a height of 15 cm.

2.5.2. Test methods

(1) Anti-icing test

The freezing interface strain generated from the freezing process was collected by an indirect method. During the test, a circular strain gauge was pasted to the center area of the uncoated aluminum surface. A volume of 20 μL of deionized water was titrated to the substrate surface by a micropipette. The freezing process of droplets is observed using the apparatus shown in Fig. 2 a, and the interface strain generated by the attached water during the freezing process is collected simultaneously. Meanwhile, the internal temperature of the water droplet is also measured during the freezing process. The surface temperature of the sample is changed by adjusting the operating power of the thermoelectric. During the test, the diameter of the circular strain gauge (Model: BHF350-12 KA, purchased from Taizhou Huangyan Electronic Components Co., Ltd) is 15 mm and the sensitivity factor is 2.8. The acquisition frequency of the system was set at 10 Hz.

In the test, the freezing time of water was utilized as an evaluation index for the anti-icing performance of GPSC compared to the phase change time of water on the aluminum alloy surface.

(2) De-icing test

During the present study, the de-icing test included the solar melting ice test and the electrothermal melting ice test. The ice cube of the same size as the substrate was prepared by the mold method, and the thickness of the ice cube was 3 mm. Aluminum alloy and GPSC specimens with ice on the surface were placed in a −20 °C environment and frozen for 12 h.

Aluminum alloy coated with GPSC and aluminum alloy was pasted on the electrothermal film surface using thermally conductive silicone. In the photothermal melting ice test, two specimens were irradiated using a solar simulator with a light intensity set to 1000 W/m^2. When conducting the electrothermal melting ice test, a low-power electrothermal film was powered to melt the accumulated ice. The melting process and time of the accreted ice on the GPSC surface and the aluminum alloy surface were respectively recorded.

(3) Mechanical stability test

The prepared GPSC coating was subjected to a quartz sand impact using the method shown in Fig. 2 b. The contact angle of the GPSC surface after 4 kg of quartz sand impact was measured and the microstructure of the GPSC surface was observed.

3. Results and discussion

3.1. Surface characterization

Fig. 3 shows the characterization results of the GPSC surface. The average static contact angle of water on the GPSC surface is 150.4° and the sliding angle was 2°, as shown in Fig. 3 a. It can indicate that the prepared coatings have superhydrophobic properties. Applying the coating can significantly improve the wettability compared to aluminum with hydrophilicity.

The microscopic morphology of the GPSC surface is shown in Fig. 3 b. It can be seen that the photothermal-superhydrophobic coating has a micro-scale structure with modified SiO_2 nanoparticles uniformly embedded on the structure surface. Hence, a multilevel structure is formed on the GPSC surface, which can affect the water attachment on the material surface and reduce the contact area between the water and substrate. This will cause the water attachment morphology on the GPSC surface to be approximately spherical. Meanwhile, the multilevel structure of the GPSC can enhance solar absorption [84]. The surface roughness of GPSC is 13.76 μm, and the GPSC surface has a regular microstructure, as shown in Fig. 3 c.

Fig. 3 d shows the results of the material composition analysis of GPSC. It can be seen that GPSC is mainly composed of elements such as C, H, O, F, and Si. The element F is from the FAS-17solution. The appearance of the Au element is due to the gold spraying treatment on the GPSC surface during testing. The solar absorption rate by aluminum alloy and GPSC is shown in Fig. 3 e. The orange area in Fig. 3 e is the solar energy spectrum [85]. The solar absorption by GPSC is significantly higher than that of the aluminum alloy under the same light conditions. Aluminum has less than 40% solar adsorption in the visible wavelength, especially infrared light range, however, GPSC has more than 70% solar adsorption in the same range. Fig. 3 f shows the FT-IR spectra of GPSC. Multiple peaks within the range of 3400 cm^{-1} to 2200 cm^{-1} are stretching vibrations of the O–H. The peak at 1468.59 cm^{-1} is the angular vibration of the Ch_2. Multiple peaks within the range of 3400 cm^{-1} to 2200 cm^{-1} are caused by carbon-fluorine vibration. The peak at 873.05 cm^{-1} is the contraction of organosilicon Si–C, and the peak at 792.06 cm^{-1} is the symmetric stretching vibration of the quartz Si–*O*–Si.

Fig. 4 shows the temperature variations on the surface of the aluminum alloy and GPSC collected by a thermal imager under irradiation conditions with a light intensity of 1000 W/m^2. The surface temperature change of the aluminum alloy was small, while the surface temperature of GPSC increased from 24.58 °C to 61.73 °C within 300s. The growth rate of the GPSC surface temperature was more than nine times that of the aluminum alloy surface temperature.

3.2. Anti/de-icing test

3.2.1. Anti-icing test

The freezing process of water on the surface of aluminum alloy and GPSC (shown in Fig. 5) was using the device shown in Fig. 2. Although water has the same freezing process and freezing phenomenon on different surfaces with different temperatures, droplets have different

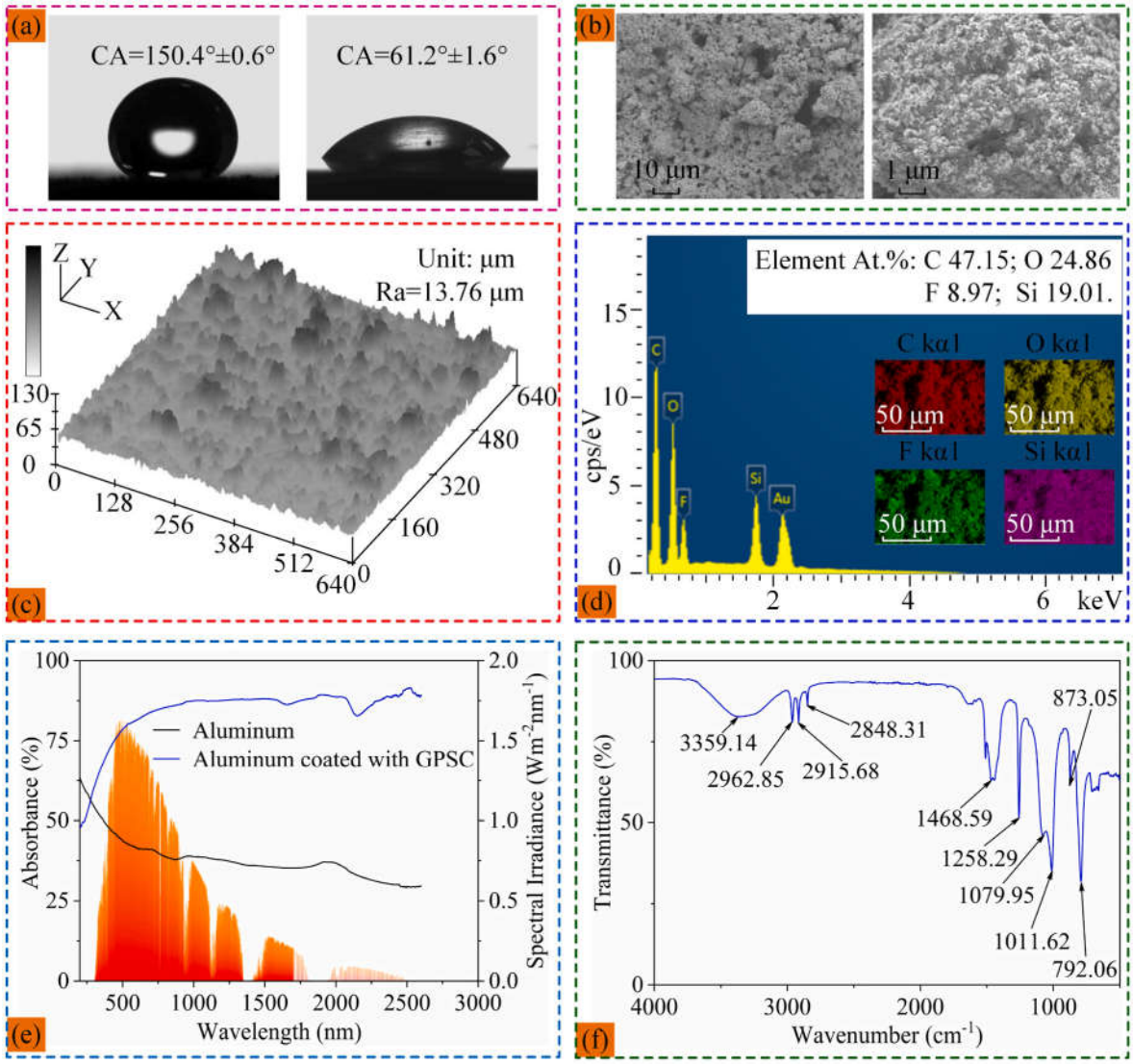

Fig. 3. Surface characterization of the prepared coatings. (a) and (b) were the wettability and SEM images of the coating; (c) was the surface roughness of the GPSC coating; (d) Material composition analysis of modified SiO_2; (e) were the light absorbance of aluminum without and with GPSC coating; (f) was the infrared spectrum of the GPSC coating.

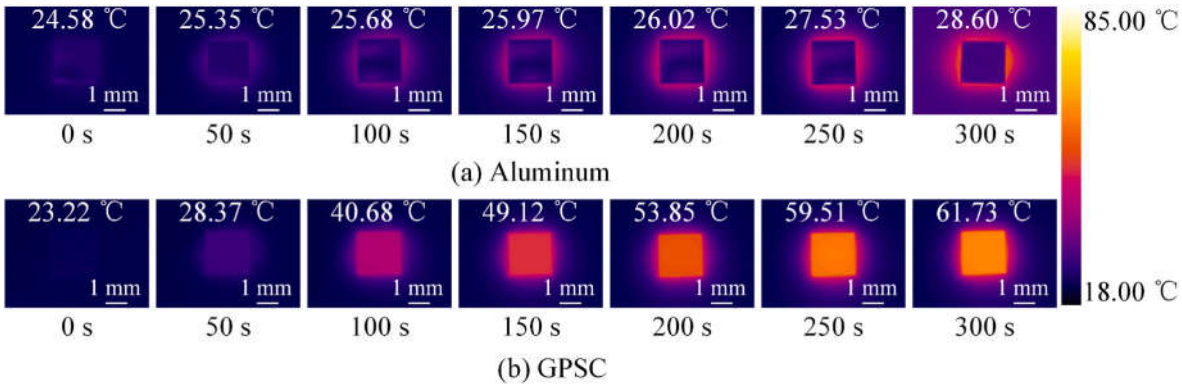

Fig. 4. Photothermal properties of different surfaces.

attachment morphology on aluminum alloy and GPSC. The whole freezing process can be separated into (i) supercooled state; (ii) phase state; (iii) stable state and the frosting stage. Water adhering to the aluminum alloy surface presents a hemispherical shape, while water attached to the GPSC surface approximates a sphere. Compared with the freezing time of water on the surface of aluminum alloy, the GPSC surface can delay the phase transition time of the attached water and show a good anti-icing performance. For example, the freezing time of

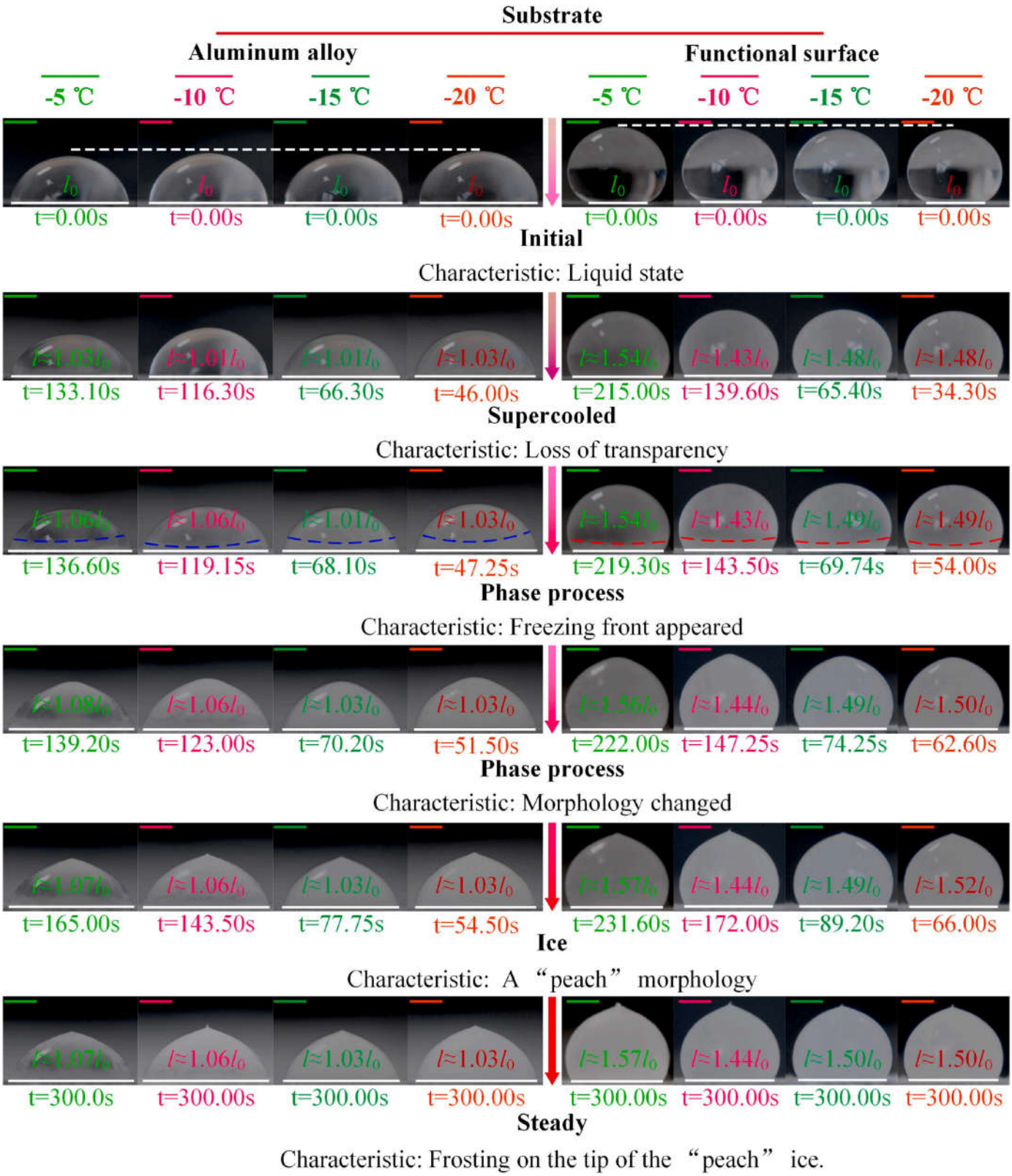

Fig. 5. Freezing processes on different substrate surfaces with different surface temperatures.

water on the GPSC surface at −5 °C is delayed by 82.70 s compared to the freezing time of water on the aluminum alloy surface.

Meanwhile, the contact diameter between water and the GPSC surface is smaller than that between water and the aluminum surface, but the height of water or ice attached to the GPSC surface is greater than that of water/ice attached to the aluminum alloy surface. Compared to the change in contact diameter between water and aluminum during the freezing process, the change in contact diameter between water and GPSC is more obvious, as shown in Fig. 5. The cold surface can restrict the spreading of the attached water on the aluminum alloy surface (as

shown in Fig. 5), so the initial height of the water gradually increases with the decrease of the target temperature. Due to the super-hydrophobic properties of the prepared coat on the substrate surface (as shown in Fig. 3 a), the contact diameter between water and the GPSC surface is reduced, the cooling rate of the cold surface on the attached water is decreased, and the phase change time for the attached water will be delayed. So the phase transition time of water adhering to the GPSC surface is later than that of water adhering to the aluminum alloy surface.

Meanwhile, a high-speed camera was utilized to record 20 μl of water falling from a distance of 10 cm from the cold surface and impacting the GPSC surface at −20 °C. The acquisition frequency of the high-speed camera was set to 2000 frames/second. Fig. 6 shows the process of water droplets impacting the GPSC surface. When the droplet approaches the cold surface, the contact area of water on the cold surface could spread first to the maximum and then shrink to the minimum, as shown in Fig. 6 a to Fig. 6 f. At this point, the droplet shape was elongated (as shown in Fig. 6 g). Water began to bounce at the highest point re-drop onto the GPSC surface, spread on the GPSC surface to a maximum area, and then retracted, as shown in Fig. 6 g to Fig. 6 k. After multiple bounces, the bounced height of the water gradually decreased, and the droplets could no longer jump off the GPSC. A stable state of water would not reach and the droplets could be rolling off the material surface, as shown in Fig. 6 l to Fig. 6 r.

The gravitational potential energy gained by the water is converted into kinetic potential energy when it drops from a high location onto a cold surface. When the water spreads on the GPSC surface, the resistance such as contact line friction, viscous loss, air resistance, electrostatic force, and other forces, can be overcome [86]. The GPSC surface with a low temperature will reduce the internal kinetic energy of the attached water during the spreading process. Moreover, the surface tension of water will also restrict the droplets from spreading on the material surface during the spreading process. Water will also need to overcome gravitational potential energy when the droplets rebound.

Meanwhile, the freezing interface strain between water and material during the freezing process was collected synchronously using a self-built device shown in Fig. 2 a. The experimental results are shown in Fig. 7. At low temperatures, metal substrates will shrink and water will phase into ice accompanied by an increase in volume (as shown in Fig. 5). Water can undergo the phase transition and volume expansion, increasing the contact diameter between water and the substrate (as shown in Fig. 5). Therefore, the freezing interface strain between water

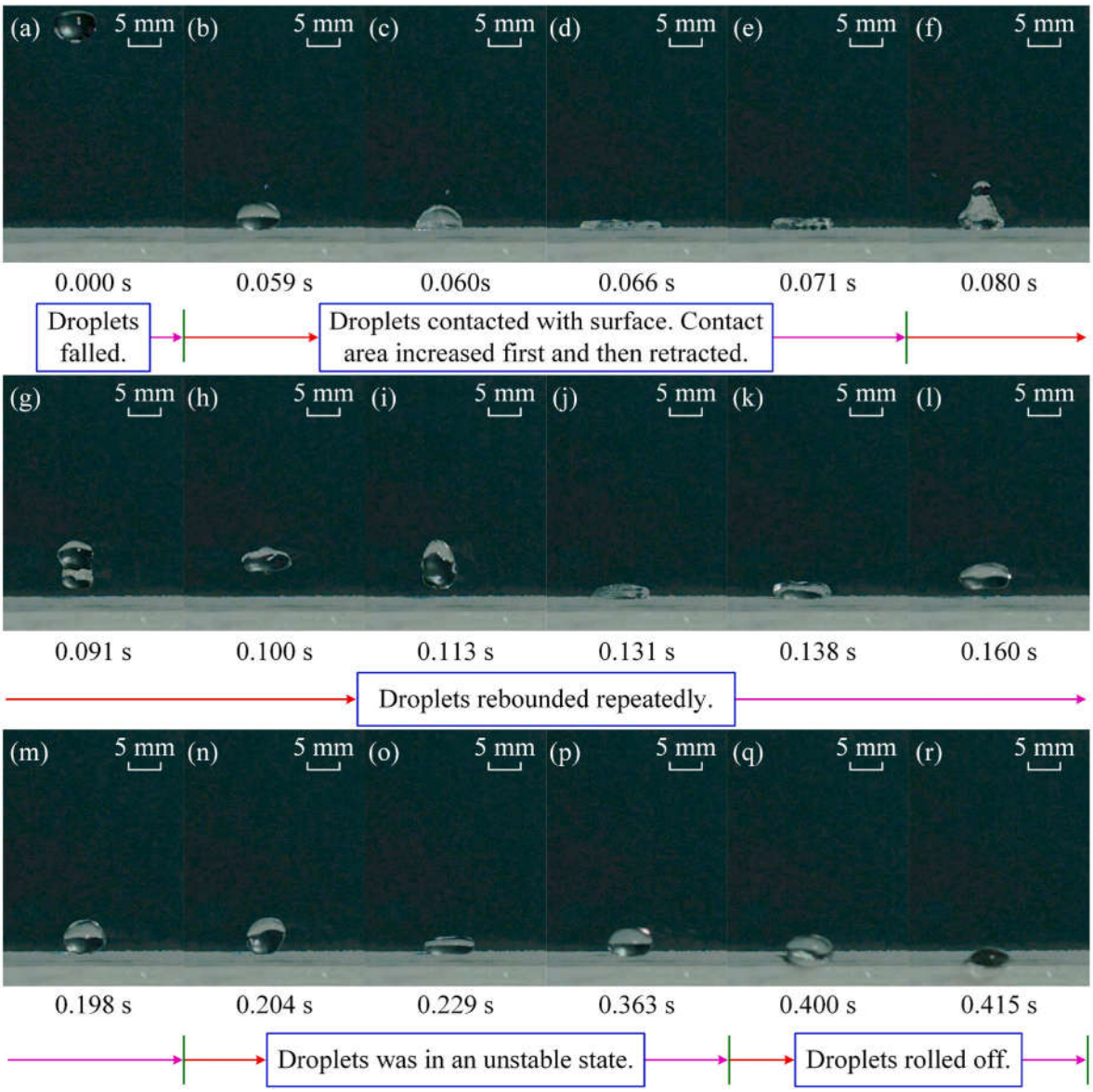

Fig. 6. Bouncing of droplets on the GPSC surface with −20 °C.

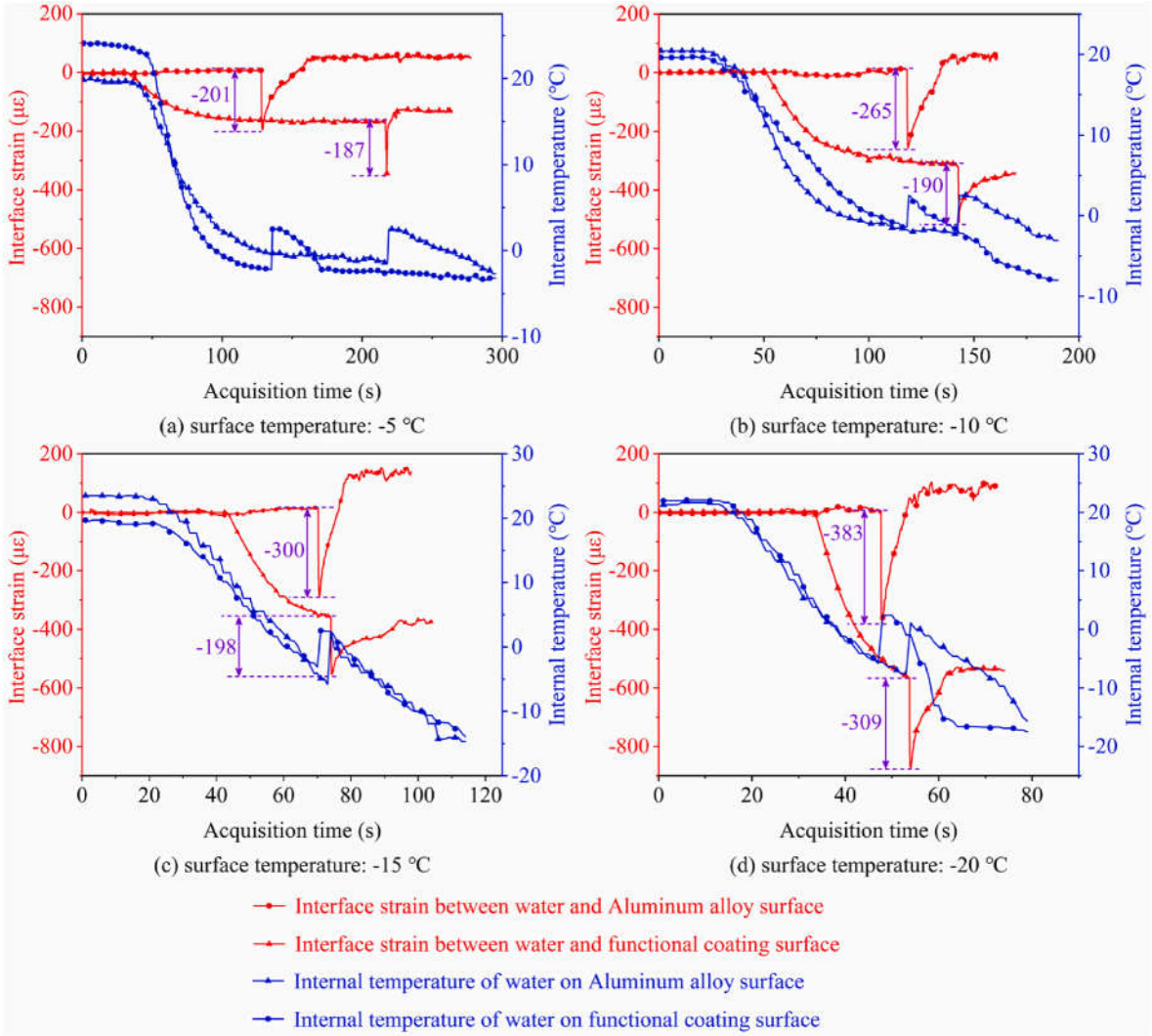

Fig. 7. Freezing process of water on the surface of aluminum and coating and the changes in interfacial strain during the freezing process.

and substrate will change in low-temperature environments. The interface strain will change abruptly when the phase transition of the attached water occurs, and the growth values increase gradually as the substrate surface temperature decreases. As shown in Fig. 7, the maximum strains formed by the adhering water during the phase transformation of aluminum alloy surfaces at −5 °C, 10 °C, −15 °C, and −20 °C are 201, 265, 300, and 383, respectively. As shown in Fig. 5, compared to the initial contact diameter, the change in contact diameter between water and GPSC during the freezing process is more significant than that of the contact diameter between water droplets and aluminum. The time when the attached water is in a supercooled state on the GPSC surface is greater than that of the attached water on the aluminum alloy surface. It will result in a sudden change in interfacial strain caused by water adhering to the GPSC surface during the freezing process, which occurs later than the sudden change in interfacial strain caused by water on the aluminum alloy surface and will slowly act on the frozen interface. Under the same conditions, the interface strain generated by water adhesion on the GPSC surface will be lower than that generated by water adhesion on the aluminum alloy surface. Therefore, the variation law of interface strain during the freezing process of water on the GPSC surface is different from that of interface strain during the freezing process of water on the aluminum alloy surface.

It is well known that the ice adhesion strength on the material surface increases with decreasing ambient temperature [87,88]. Hence, timely intervention in the freezing process of the attached water and removal of the accreted ice from the material surface when the ice adhesion strength was lowest can minimize the ice adhesion hazards and reduce the anti/de-icing cost. Based on the experimental results shown in Fig. 7, it can be seen that whether water freezes on the aluminum alloy surface or the superhydrophobic surface, the interface strain generated from the freezing process will change abruptly. By monitoring the change of the freezing interface strain between water and material, it is possible to monitor the state of the attached water as well as to determine the phase change in real-time. Utilizing the characteristics of the freezing process can provide experimental support for the execution time of the active anti/de-icing methods, such as mechanical, thermal, and chemical methods, as well as a theoretical basis for developing a new kind of anti/de-icing control system.

3.2.2. *De-icing test*

Fig. 8 shows the solar melting process of the accumulated ice on aluminum and GPSC surfaces at −20 °C. When GPSC completely melted the covered ice within 445.60s, the accreted ice on the aluminum alloy surface was not been melted under the same light intensity, as shown in Fig. 8 a and Fig. 8 f. This indicated that the GPSC surface has a good solar energy absorption performance, which is consistent with the experimental results shown in Fig. 3 e. As the illumination time prolongs, the edge area of the accumulated ice on the GPSC surface gradually begins to melt, and the melted water starts to drip down, as shown in Fig. 8 g to Fig. 8 i. Due to the superhydrophobicity of the GPSC surface, the melted

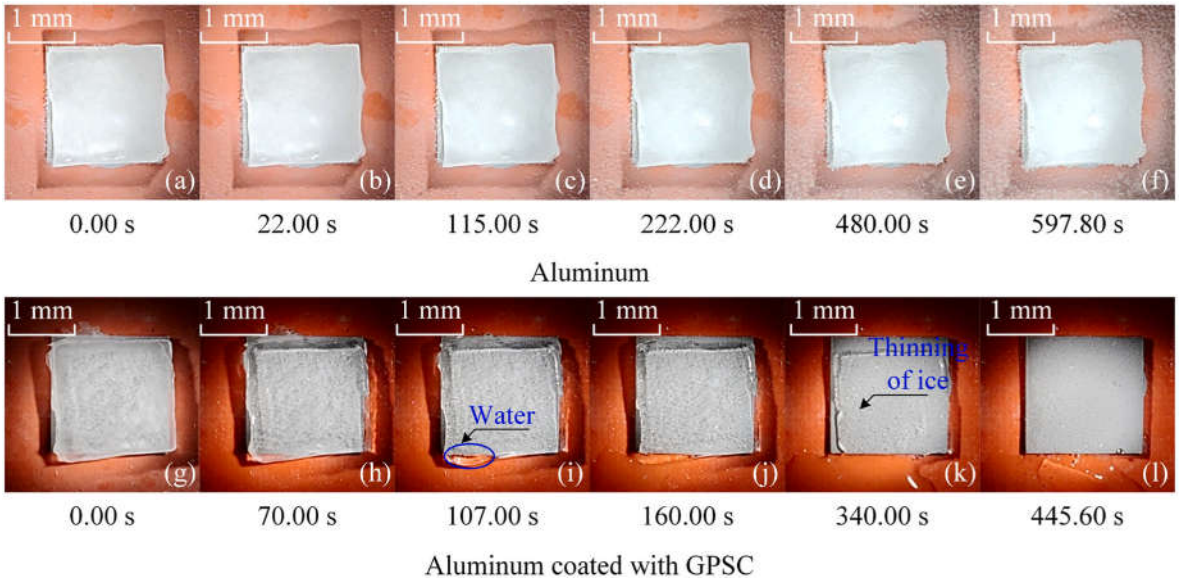

Fig. 8. Photothermal melting ice tests.

water will drive the accumulated ice to slide on the GPSC surface. With the continued illumination, the amount of melting water on the GPSC surface gradually increased, and the accreted ice began to thin until it was completely melted, as shown in Fig. 8 j to Fig. 8 l.

Fig. 9 shows the thermal melting process of the accumulated ice on the surface of aluminum alloy and GPSC at a surface temperature of −20 °C after the electrothermal film is energized. Since GPSC is mainly composed of graphene, it will enhance the electrical and thermal conductivity of GPSC. Compared to the electrothermal melting process time of 613.00 s for the accreted ice on the aluminum alloy surface, the electrothermal melting process time of the attached ice on the GPSC surface was reduced by 341.00 s. The time to melt the ice on the GPSC surface was reduced by 55.63% compared to the time required to melt ice adhered to the aluminum alloy surface. It can be seen that GPSC has good electrothermal ice melting performance. During the electrothermal ice melting test, the water from the melting ice on the aluminum alloy surface adheres to the material surface without rolling off, as shown in Fig. 9 a to Fig. 9 f. However, water from melting ice attached to the GPSC surface rolls from the material surface under the effect of superhydrophobicity, s shown in Fig. 9 g to Fig. 9 l. It will also drive the accumulated ice to slide on the GPSC surface, as shown in Fig. 9 k.

The energy consumption of electrothermal ice melting on the aluminum alloy is 55.63% higher than that of melting the ice on the GPSC surface. During the test, the power of the electrothermal film is 9W and the size of the ice overlay is 20 mm × 20 mm × 1 mm (L × W × H). If the time without sunlight is hours, the electric heating film needs to consume energy of about 210 kJ to melt the accumulated ice on the GPSC surface. 1 m^2 of solar PV panels can produce 3600 W per day under normal conditions [89,90]. Therefore, 1 m^2 of solar PV panels can fully satisfy the energy consumption of melting large areas of the accreted ice on the GPSC surface.

3.2.3. *Mechanical ability test*

The GPSC surface was impacted with 4 kg of quartz sand by utilizing the device shown in Fig. 2 b. The contact angle of the GPSC surface impacted by quartz sand was measured, as shown in Fig. 10 a. The

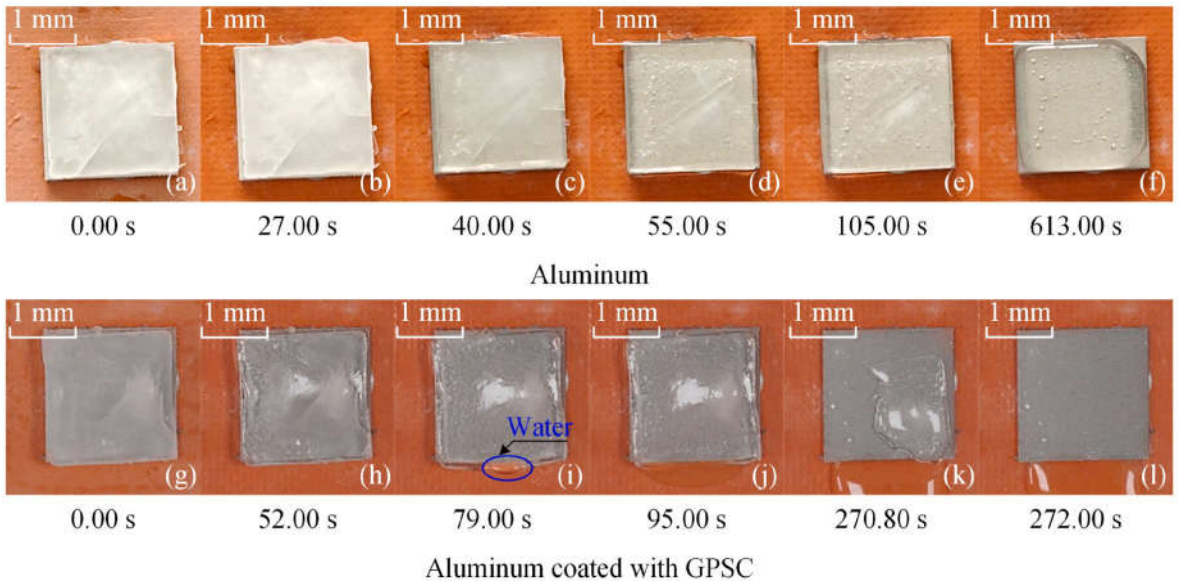

Fig. 9. Electrothermal ice melting tests.

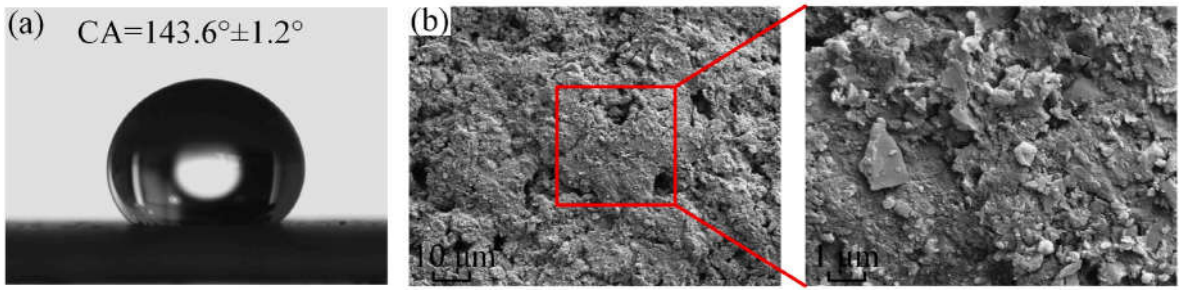

Fig. 10. Sand impact test. (a) and (b) were respective the contact angle and the SEM image of GPSC after sand impact.

contact angle of water on the GPSC surface impacted by quartz sand is 143.6°, which still has good hydrophobicity, but the sliding angle of the GPSC surface is greater than 10°. Fig. 10 b shows the microstructure of the GPSC surface after quartz sand impact. After 4 kg of quartz sand impact, some of the SiO_2 adhering to the GPSC surface was taken away, resulting in a decrease in the wettability of the GPSC surface.

4. Conclusions

During the present study, an all-weather anti/de-icing method was proposed to realize the removal of the accumulated ice on the material surface through a combination of passive and active methods. An anti/de-icing coating with excellent light absorption and superhydrophobic characteristics was applied to enhance the passive anti-icing performance of the surface under sunlight, and low-power electrothermal was used to melt the overlying ice on the surface at dark.

The average contact angle of water on the GPSC surface is 150.4° with a sliding angle is 2°, with good solar absorption property at visible and infrared light ranges. The freezing time of water on the aluminum alloy surface of −5 °C is 82.70 s more than that on the GPSC surface. Under the same illumination intensity, the surface temperature of GPSC rises to 61.73 °C and the covered ice can be completely melted within 445.60 s, while the accreted ice on the aluminum alloy surface does not melt. The water rolling off formed by the melting ice on the GPSC surface with superhydrophobic characteristics can achieve surface self-cleaning and avoid secondary freezing. When conducting electrothermal ice melting tests, the melting time of the accumulated ice on the GPSC surface was reduced by 55.63% compared to the melting time of the accumulated ice on the aluminum alloy surface. After 4 kg of quartz sand impact, the surface of GPSC still has good hydrophobicity with a contact angle of 143.6°.

Moreover, it is found that a sudden change in the freezing interface strain between water and the material during the freezing process. The interface strain gradually increases with the decrease in ambient temperature, but it can be reduced by the delayed effect of the superhydrophobic coating on the freezing of the attached water. For example, the attached water forms an interfacial strain of 383 on the aluminum alloy at −20 °C, but an interfacial strain of 309 on the aluminum alloy with a photothermal superhydrophobic coating. Based on the change of the interface strain, it can provide a new icing monitoring method for the engineering field, as well as a reference and theoretical basis for the implementation time of existing anti/de-icing methods. Of course, follow-up research will be carried on about the development of new icing monitoring techniques.

The present study can provide a new all-weather anti/de-icing method for the engineering field. When the photothermal-superhydrophobic coating is illuminated, the anti/de-icing purpose of the material can be achieved by spraying the GPSC on the material; in the absence of sunlight, the energy consumption of removing the accreted ice by electrothermal de-icing methods will be reduced due to the thermal and electrical conductivity of the GPSC. Furthermore, it can provide a reference for icing monitoring technology in the engineering field as well as for the start of operation time of anti/de-icing methods.

Data availability

No data was used for the research described in the article.

Declaration of competing interest

The authors declare that they have no known competing financial interests or personal relationships that could have appeared to influence the work reported in this paper.

Acknowledgments

This work was supported by the National Natural Science Foundation of China (Grant No. 52205309), the Department of Science and Technology of Jilin Province, China (Grant No. 20220101215JC), the Sichuan Province All-electric Navigation Aircraft Key Technology Engineering Research Center (Grant No. CAFUC202401KF001), and Key Laboratory of Icing and Anti/De-icing (Grant No. IADL20230104).

References

[1] Xie ZT, Wang H, Geng Y, Li M, Deng QY, Tian Y, Chen R, Zhu X, Liao Q. Carbon-based photothermal superhydrophobic materials with Hierarchical structure enhances the anti-icing and photothermal deicing properties. ACS Appl Mater Interfaces 2021;13:4308–48321. https://doi.org/10.1021/acsami.1c15028.
[2] Yirtici O, Tuncer IH. Aerodynamic shape optimization of wind turbine blades for minimizing power production losses due to icing. Cold Reg Sci Technol 2021;185:103250. https://doi.org/10.1016/j.coldregions.2021.103250. ID.
[3] Swenson L, Gao L, Hong J, Shen L. An efficacious model for predicting icing-induced energy loss for wind turbines. Appl Energy 2022;305:117809. https://doi.org/10.1016/j.apenergy.2021.117809. ID.
[4] Parent O, Ilinca A. Anti-icing and de-icing techniques for wind turbines: critical review. Cold Reg Sci Technol 2011;65:88–96. https://doi.org/10.1016/j.coldregions.2010.01.005.
[5] Roberge P, Lemay J, Ruel J, Begin-Drolet A. Evaluation of meteorological measurements made on the nacelle of wind turbines in cold climate. Cold Reg Sci Technol 2022;203:103658. https://doi.org/10.1016/j.coldregions.2022.103658. ID.
[6] Wei KX, Yang Y, Zuo HY, Zhong DD. A review on ice detection technology and ice elimination technology for wind turbine. Wind Energy 2020;23:433–57. https://publons.com/publon/10.1002/we.2427.
[7] Gui K, Liu JY, Ge JF, Li HY, Ye L. Atmospheric icing process measurement utilizing impedance spectroscopy and thin film structure. Measurement 2022;202:111851. https://doi.org/10.1016/j.measurement.2022.111851. ID.
[8] Zhang ZH, Zhou WS, Li H. Icing estimation on wind turbine blade by the interface temperature using distributed fiber optic sensors. Struct Control Health Monit 2020;27:2534. https://doi.org/10.1002/stc.2534. ID.
[9] Jin XH, Zhang XY, Cheng X, Jiang GQ, Masisi L, Huang W. A Physics-based and data-driven Feature Extraction model for blades icing detection of wind turbines. IEEE Sens. J. 2023;23:3994. https://doi.org/10.1109/JSEN.2023.3234151. 3954.
[10] Lamraoui F, Fortin G, Benoit R, Perron J, Masson C. Atmospheric icing impact on wind turbine production. Cold Reg Sci Technol 2014;100:36–49. https://doi.org/10.1016/j.coldregions.2013.12.008.
[11] Lin YB, Chen HF, Wang GY, Liu AH. Recent progress in Preparation and anti-icing applications of superhydrophobic coatings. Coatings 2018;8:208. https://doi.org/10.3390/coatings8060208. ID.
[12] Guo HS, Liu M, Xie CH, Zhu YN, Sui XJ, Wen CY, Li QS, Zhao WQ, Zhang L, Yang J. A sunlight-responsive and robust anti-icing/deicing coating based on the

amphiphilic materials. Chem Eng J 2020;402:126161. https://doi.org/10.1016/j.cej.2020.126161. ID.
[13] Wang ZJ. Recent progress on ultrasonic de-icing technique used for wind power generation, high-voltage transmission line and aircraft. Energy Build 2017;140:42–9. https://doi.org/10.1016/j.enbuild.2017.01.072.
[14] Zhu YC, Huang XB, Jia JY, Tian Y, Zhao L, Zhang Y, Cui YT, Li XB. Experimental study on the thermal conductivity for transmission line icing. Cold Reg Sci Technol 2016;129:96–103. https://doi.org/10.1016/j.coldregions.2016.06.009.
[15] Jin JF, Chen YY, Qi YC, Cong Q, Chen TK, Choy KL, Ren LQ. Changes in the interfacial stress of water on aluminum alloy surface during the freezing and thawing process. Cold Reg Sci Technol 2022;194:103460. https://doi.org/10.1016/j.coldregions.2021.103460. ID.
[16] Jin JF, Chen YY, Chen TK, Qi YC, Cong Q, Liu CZ. Formation mechanism of freezing interface strain and effect of different factors on freezing interface strain. Int J Therm Sci 2023;185. https://doi.org/10.1016/j.ijthermalsci.2022.108090. ID 108090.
[17] Chen TK, Dong XJ, Han LM, Cong Q, Qi YC, Jin JF, Liu CZ, Wang MQ. Changing the freezing interface characteristics to reduce the ice adhesion strength. Appl Therm Eng 2023;230. https://doi.org/10.1016/j.applthermaleng.2023.120796. ID 120976.
[18] Andenæs E, Jelle BP, Ramlo K, Kolås T, Selj J, Foss SE. The influence of snow and ice coverage on the energy generation from photovoltaic solar cells. Sol Energy 2018;159:318–28. https://doi.org/10.1016/j.solener.2017.10.078.
[19] Wang L, Li JX, Chen ZC, Song ZT, Meng X, Chen XM. Porous graphene-based photothermal superhydrophobic surface for robust anti-icing and efficient de-icing. Adv Mater Interfac 2022;9:2201758. https://doi.org/10.1002/admi.202201758. ID.
[20] Xing QQ, Gu YX, Han Y, Li SP, Wang B, Li YQ, He GX. Experimental evaluation of the frost suppression performance of a superhydrophobic finned tube heat exchanger. Int J Heat Fluid Flow 2024;109:109497. https://doi.org/10.1016/j.ijheatfluidflow.2024.109497. ID.
[21] Gao RM, Song MJ, Chao Christopher Yu H, Lin SL, Zhang L, Zhang X. Review on condensation frosting and defrosting experiments for superhydrophobic surfaces. Appl Therm Eng 2024;236:121691. https://doi.org/10.1016/j.applthermaleng.2023.121691. ID.
[22] Li PH, Li ZL, Han ZL, Zhu SY, Zhai WM, Lou HB. Running safety evaluation of high-speed train subject to the impact of floating ice collision on bridge piers. Proc Inst Mech Eng - Part F J Rail Rapid Transit 2022;236:220–33. https://doi.org/10.1177/0954409721101000.
[23] Liu MY, Wang JB, Zhu HF, Krajnovic S, Zhang Y, Gao GK. A numerical study on water spray from wheel of high-speed train. J Wind Eng Ind Aerod 2020;197:104086. https://doi.org/10.1016/j.jweia.2019.104086. ID.
[24] Zhang YJ, Liu ZD, Stichel S. Study on the braking distance of composite brake blocks covered with ice for freight trains in winter. Proc Inst Mech Eng - Part F J Rail Rapid Transit 2023;237:1050–9. https://doi.org/10.1177/09544097231151474.
[25] Tan Z, Gou HY, Li WH, B Y. Effect of frost heave deformation of bridge foundation on operation safety of high-speed railway. Structures 2023;47:2099–112. https://doi.org/10.1016/j.istruc.2022.12.011.
[26] Wang JB, Zhang J, Xie F, Zhang Y, Gao GJ. A study of snow accumulating on the bogie and the effects of deflectors on the de-icing performance in the bogie region of a high-speed train. Cold Reg Sci Technol 2018;148:121–30. https://doi.org/10.1016/j.coldregions.2018.01.010.
[27] Borrebæk POA, Jelle BP, Zhang ZL. Avoiding snow and ice accretion on building integrated photovoltaics-challenges, strategies, and opportunities. Sol Energy Mater Sol Cells 2020;206:110306. https://doi.org/10.1016/j.solmat.2019.110306. ID.
[28] He Q, Li KS, Xu ZH, Wang JW, Wang XS, Li AL. Research progress on construction strategy and technical evaluation of aircraft icing accretion protection system. Chin J Aeronaut 2023;36:1–23. https://doi.org/10.1016/j.cja.2023.07.003.
[29] Samuelsen EM, Graversen RG. Weather situation during observed ship-icing events off the coast of northern Norway and the Svalbard archipelago. Weather Clim Extrem 2019;24:100200. https://doi.org/10.1016/j.wace.2019.100200. ID.
[30] Andenæs E, Jelle BP, Ramlo K, Kolås T, Selj J, Foss SE. The influence of snow and ice coverage on the energy generation from photovoltaic solar cells. Sol Energy 2018;159:318–28. https://doi.org/10.1016/j.solener.2017.10.078.
[31] Dehghani-Sanij AR, Dehghani SR, Naterer GF, Muzychka YS. Marine icing phenomena on vessels and offshore structures: prediction and analysis. Ocean Eng 2017;143:1–23. https://doi.org/10.1016/j.oceaneng.2017.07.049.
[32] Borrebæk POA, Jelle BP, Zhang ZL. Avoiding snow and ice accretion on building integrated photovoltaics-challenges, strategies, and opportunities. Sol Energy Mater Sol Cells 2020;206:110306. https://doi.org/10.1016/j.solmat.2019.110306. ID.
[33] Samuelsen EM, Graversen RG. Weather situation during observed ship-icing events off the coast of northern Norway and the Svalbard archipelago. Weather Clim Extrem 2019;24:100200. https://doi.org/10.1016/j.wace.2019.100200. ID.
[34] Kolbakir C, Hu HY, Liu Y, Hu H. An experimental study on different plasma actuator layouts for aircraft icing mitigation. Aero Sci Technol 2020;107:106325. https://doi.org/10.1016/j.ast.2020.106325. ID.
[35] Shen YZ, Wu XH, Tao J, Zhu CL, Lai YK, Chen Z. Superhydrophobic coating for blade surface ice-phobic properties of wind turbines: a review. Prog Mater Sci 2024;187:108145. https://doi.org/10.1016/j.porgcoat.2023.108145. ID.
[36] Yancheshme AA, Momen G, Aminabadi RJ. Mechanisms of ice formation and propagation on superhydrophobic surfaces: a review. Adv Colloid Interface Sci 2020;197:102155. https://doi.org/10.1016/j.cis.2020.102155. ID.
[37] Guerin F, Laforte C, Farinas MI, Perron J. Analytical model based on experimental data of centrifuge ice adhesion tests with different substrates. Cold Reg Sci Technol 2016;121:9–99. https://doi.org/10.1016/j.coldregions.2015.10.011.
[38] Jung S, Tiwari MK, Doan NV, Poulikakos D. Freezing-induced wetting transitions on superhydrophobic surfaces. Nat Commun 2012;3:615. https://doi.org/10.1038/ncomms1630. ID.
[39] Memon H, Liu JP, De Focatiis DSA, Choi KS, Hou XH. Intrinsic dependence of ice adhesion strength on surface roughness. Surf Coat Technol 2020;185:125382. https://doi.org/10.1016/j.surfcoat.2020.125382. ID.
[40] Emelyanenko KA, Emelyanenko AM, Boinovich LB. Water and ice adhesion to solid surfaces: common and specific, the impact of temperature and surface wettability. Coatings 2020;10:648. https://doi.org/10.3390/coatings10070648. ID.
[41] Zhao J, Wang XC, Zhou B, Wu WJ, Zheng WH, Yuan C. Influence of surface characteristics of cement pavement on ice-concrete adhesion. Construct Build Mater 2023;394:132259. https://doi.org/10.1016/j.conbuildmat.2023.132259. ID.
[42] Janjua ZZ. The influence of freezing and ambient temperature on the adhesion strength of ice. Cold Reg Sci Technol 2017;140:14–9. https://doi.org/10.1016/j.coldregions.2017.05.001. ID.
[43] Chen TK, Cong Q, Sun CB, Jin JF, Choy KL. Influence of substrate initial temperature on adhesion strength of ice on aluminum alloy. Cold Reg Sci Technol 2018;148:142–7. https://doi.org/10.1016/j.coldregions.2018.01.017.
[44] Xue XF, Qiang GY, Feng YW, Luo TS. Experimental study on the adhesion strength of the frozen ice for aircraft moving parts. Aerospace 2022;9(10):589. https://doi.org/10.3390/aerospace9100589.
[45] Zhang YJ, Guo RZ, Zhang YH, Liang K. Adhesion shear strength test method for freshwater/seawater ice on carbon ceramic brake pads of amphibious aircraft. Aircraft Eng Aero Technol 2022;94:781–91. https://doi.org/10.1108/AEAT-01-2021-0019.
[46] Luo WT, Zarasvand KA, Dijvejin ZA, Nadaraja AV, Golovin K. Influence of salinity on surface ice adhesion strength. Adv Mater Interfac 2024;11:230066. https://doi.org/10.1002/admi.202300606. ID.
[47] Tian Z, Wang LZ, Zhu DY, Chen CH, Zhao HY, Peng R, Zhang HJ, Fan PX, Zhong ML. Passive anti-icing performances of the same superhydrophobic surfaces under static freezing, dynamic supercooled-droplet impinging, and icing wind tunnel tests. ACS Appl Mater Interfaces 2023;15(6013):6013–24. https://doi.org/10.1021/acsami.2c15253.
[48] Rekuviene R, Saeidiharzand S, Mazeika L, Samaitis V, Jankauskas A, Sadaghiani AK, Gharib G, Muganli Z, Kosar A. A review on passive and active anti-icing and de-icing technologies. Appl Therm Eng 2024;250:123474. https://doi.org/10.1016/j.applthermaleng.2024.123474. ID.
[49] Wu BR, Cui X, Jiang HY, Wu N, Peng CY, Hu ZF, Liang XB, Yan YG, Huang J, Li DS. A superhydrophobic coating harvesting mechanical robustness, passive anti-icing and active de-icing performances. J Colloid Interface Sci 2021;590:301–10. https://doi.org/10.1016/j.jcis.2021.01.054.
[50] He ZW, Xie HM, Jamil MI, Li T, Zhang QH. Electro-/Photo-Thermal promoted anti-icing materials: a new strategy combined with passive anti-icing and active de-icing. Adv Mater Interfac 2022;9:2200275. https://doi.org/10.1002/admi.202200275. ID.
[51] Parent O, Ilinca A. Anti-icing and de-icing techniques for wind turbines: critical review. Cold Reg Sci Technol 2011;65:88–96. https://doi.org/10.1016/j.coldregions.2010.01.005.
[52] Hao L, Li QY, Pan WC, Li BL. Icing detection and evaluation of the electro-impulse de-icing system based on infrared images processing. Infrared Phys Technol 2020;109:103424. https://doi.org/10.1016/j.infrared.2020.103424. ID.
[53] Li LK, Liu Y, Tian LC, Hu HY, Hu H, Liu XJ, Kohli A. An experimental study on a hot-air-based anti-/de-icing system for aero-engine inlet guide vanes. Appl Therm Eng 2020;167:114778. https://doi.org/10.1016/j.applthermaleng.2019.114778. ID.
[54] Zhang Z, Chen BB, Lu CD, Wu HL, Wu HP, Jiang SF, Chai GZ. A novel thermo-mechanical anti-icing/de-icing system using bi-stable laminate composite structures with superhydrophobic surface. Compos Struct 2017;180:933–43. https://doi.org/10.1016/j.compstruct.2017.08.068.
[55] Tarfaoui M, El Moumen A, Boehle M, Shah O, Lafdi K. Self-heating and deicing epoxy/glass fiber based carbon nanotubes buckypaper composite. J Mater Sci 2019;54:1351–62. https://doi.org/10.1007/s10853-018-2917-9.
[56] Golovin K, Dhyani A, Thouless MD, Tuteja A. Low-interfacial toughness materials for effective large-scale deicing. Science 2019;364:371–5. https://www.science.org/doi/10.1126/science.aav1266.
[57] Shen YZ, Wu XH, Tao J, Zhu CL, Lai YK, Chen Z. Icephobic materials: fundamentals, performance evaluation, and applications. Prog Mater Sci 2019;103:509–57. https://doi.org/10.1016/j.pmatsci.2019.03.004.
[58] Yang PY, Yin K, Song XH, Wang LX, Deng QW, Pei JQ, He YC, Arnusch CJ. Triggered water film self-sculpturing on femtosecond laser-induced heterogeneously wetted micro/nanostructured surfaces. Nano Lett 2024;24(10):3133–41. https://doi.org/10.1021/acs.nanolett.3c05042.
[59] He YC, Yin K, Wang LX, Wu TN, Chen Y, Arnusch CJ. Femtosecond laser structured black superhydrophobic cork for efficient solar-driven cleanup of crude oil. Appl Phys Lett 2024;124(17):171601. https://doi.org/10.1063/5.0199291. ID.
[60] Wu TN, Yin K, Pei JQ, He YC, Duan JA, Arnusch CJ. Femtosecond laser-textured superhydrophilic coral-like structures spread AgNWs enable strong thermal camouflage and anti-counterfeiting. Appl Phys Lett 2024;124(16):161602. https://doi.org/10.1063/5.0190986. ID.
[61] Wang LX, Yin K, Deng QW, Huang QQ, Arnusch CJ. Multiscale hybrid-structured femtosecond laser-induced graphene with outstanding photo-electro-thermal

effects for all-day anti-icing/deicing. Carbon 2024;219:118824. https://doi.org/10.1016/j.carbon.2024.118824. ID.
[62] Tian XL, Verho T, Ras RHA. Moving superhydrophobic surfaces toward real-world applications. Science 2016;352:142–3. https://www.science.org/doi/10.1126/science.aaf2073.
[63] Milionis A, Loth E, Bayer IS. Recent advances in the mechanical durability of superhydrophobic materials. Adv Colloid Interface Sci 2016;229:57–79. https://doi.org/10.1016/j.cis.2015.12.007.
[64] Zhuo Y, Håkonsen V, He Z, Xiao S, He J, Zhang Z. Enhancing the mechanical durability of icephobic surfaces by introducing autonomous self-healing function. ACS Appl Mater Interfaces 2018;10:11972–8. https://doi.org/10.1021/acsami.8b01866.
[65] Boinovich LB, Emelyanenko AM, Emelyanenko KA, Modin EB. *Modus operandi* of protective and anti-icing mechanisms underlying the design of longstanding outdoor icephobic coatings. ACS Nano 2019;13:4335–46. https://doi.org/10.1021/acsnano.8b09549.
[66] Lu Y, Sathasivam S, Song JL, Crick CR, Carmalt CJ, Parkin IP. Robust self-cleaning surfaces that function when exposed to either air or oil. Science 2015;347:1132–5. https://www.science.org/doi/10.1126/science.aaa0946.
[67] Zhang WB, Xiang TH, Liu F, Zhang M, Gan WT, Zhai XL, Di X, Wang YZ, Liu GX, Wang CY. Facile design and fabrication of superwetting surfaces with excellent wear-resistance. ACS Appl Mater Interfaces 2017;9:15776–84. https://doi.org/10.1021/acsami.7b02158.
[68] Geng Z, He JH. An effective method to significantly enhance the robustness and adhesion-to-substrate of high transmittance superamphiphobic silica thin films. J Mater Chem A 2014;2:16601–7. https://doi.org/10.1039/C4TA03533J.
[69] Kulinich, S. A., Farhadi, S., Nose, K., Du, X. W. Superhydrophobic surfaces: are they really ice-repellent? Langmuir.201, 27, 25-29. https://doi.org/10.1021/la104277q.
[70] Li M, Liu WQ, Yin ZZ, Yang HT, Chen YH, Yang CG, Luo YD, Hong Z, Xie C, Xue MS. Facile fabrication of superhydrophobic and photocatalytic self-cleaning flexible strain sensor membrane for human motion. Sens. Actuator A-Phys. 2023;363:114750. https://doi.org/10.1016/j.sna.2023.114750. ID.
[71] Yang GY, Yin ZZ, Zha QD, Wang RT, Xie Y, Chen YH, Hong Z, Luo YD, Xue MS. A typha orientalis-inspired 3D Janus solar evaporator with controllable wettability for highly efficient and stable solar desalination. Desalination 2024;595:118318. https://doi.org/10.1016/j.desal.2024.118318. ID.
[72] Zha QD, Yao YK, Yin ZZ, Deng YT, Li ZH, Xie Y, Chen YH, Yang CG, Luo YD, Xue MS. Facile construction of multifunctional 3D smart MOF-based polyurethane sponges with photocatalytic ability for efficient separation of oil-in-water emulsions and co-existing organic pollutant. Chem Eng J 2024;490:151747. https://doi.org/10.1016/j.cej.2024.151747. ID.
[73] Deng YT, Du F, Chen ZB, Lv PY, Yin ZZ, He M, Xue MS, Li HY. Functionalized superhydrophobic coatings with electro-photothermal effect for all-day durable anti-icing. Adv Mater Interfac 2024;11(11):2300869. https://doi.org/10.1002/admi.202300869. ID.
[74] Li M, Xiao WB, Yin ZZ, Chen YH, Luo YD, Hong Z, Xue MS. Construction of a robust MOF-based superhydrophobic composite coating with the excellent performance in antifouling, drag reduction, and organic photodegradation. Prog Org Coating 2024;186:108086. https://doi.org/10.1016/j.porgcoat.2023.108086. ID.
[75] Yin ZZ, Yuan F, Xue MS, Xue YH, Xie Y, Ou JF, Luo YD, Hong Z, Xie C. A multifunctional and environmentally safe superhydrophobic membrane with superior oil/water separation, photocatalytic degradation and anti-biofouling performance. J Colloid Interface Sci 2022;611:93–104. https://doi.org/10.1016/j.jcis.2021.12.070.
[76] Deng YT, Li ZH, Yin ZZ, Chen YH, Yang CG, Luo YD, Xue MS. A facile method for constructing scalable and low-cost superhydrophobic coating with anti-corrosion and drag-reduction properties. Ind Crop Prod 2024;216:118732. https://doi.org/10.1016/j.indcrop.2024.118732. ID.
[77] Yang GY, Yin ZZ, Deng YT, Li ZH, Chen YH, Xiao WB, Hong Z, Luo YD, Xie C, Xue MS. Fabrication of flexible multifunctional graphene-based composite membrane with improved hydrophobicity and thermal conductivity characters for thermal management. Colloid Surf. A-Physicochem. Eng. Asp. 2025;704:135494. https://doi.org/10.1016/j.colsurfa.2024.135494. ID.
[78] Zha QD, Chen H, Yin ZZ, Deng YT, Li ZH, Chen YH, Yang CG, Yang HT, Luo YD, Xue MS. Highly thermally conductive multifunctional graphene-based composite membrane for remarkable passive heat dissipation and robust superhydrophobicity. Appl Therm Eng 2024;250:123469. https://doi.org/10.1016/j.applthermaleng.2024.123469. ID.
[79] Yang GY, Zhang YX, Yin ZZ, Deng YT, Li ZH, Xie Y, Chen YH, Yang CG, Yang HT, Luo YD, Hong Z, Xue MS. Robust mussel-inspired LBL carbon nanotube-based superhydrophobic polyurethane sponge for efficient oil-water separation utilizing photothermal effect. Fuel 2024;381:133353. https://doi.org/10.1016/j.fuel.2024.133353. ID.
[80] Deng YT, Du F, Chen ZB, Lv PY, Yin ZZ, He M, Xue MS, Li HY. Functionalized superhydrophobic coatings with electro-photothermal effect for all-day durable anti-icing. Adv Mater Interfac 2024;11(11):2300869. https://doi.org/10.1002/admi.202300869. ID.
[81] Yin ZZ, Chen XX, Chen ZB, Song HT, Lv PY, Xue MS, Li HY. Superhydrophobic photocatalytic self-cleaning nanocellulose-based strain sensor for full-range human motion monitoring. Adv Mater Interfac 2023;10(33):202300350. https://doi.org/10.1002/admi.202300350. ID.
[82] Kourougianni F, Arsalis A, Olympios A, Yiasoumas G, Konstantinou C, Papanastasiou P, Georghiou G. A comprehensive review of green hydrogen energy systems. Renew Energy 2024;231:120911. https://doi.org/10.1016/j.renene.2024.120911. ID.
[83] Li QQ, Wei XD, Wang JZ, Chao YX, Li Y, Fan HD. Enhancing battery energy storage systems for photovoltaic applications in extremely cold regions: a brief review. Energy Sustain Dev 2024;81:101517. https://doi.org/10.1016/j.esd.2024.101517. ID.
[84] Broadband light absorption enhancement in α-Si: H ultrathin film solar cells with nanophotonic light trapping structures. Mater Today Commun 2024;40:109595. https://doi.org/10.1016/j.mtcomm.2024.109595. ID.
[85] ASTM-G173. Standard Tables for Reference Solar Spectral Irradiances: Direct Normal and Hemispherical on 37° Tilted Surface [S] 2023.
[86] Schutzius TM, Jung S, Maitra T, Graeber G, Köhme M, Poulikakos D. Spontaneous droplet trampolining on rigid superhydrophobic surfaces. Nature 2015;527:82–5. https://doi.org/10.1038/nature15738.
[87] Chen TK, Jin JF, Qi YC, Tian WJ, Cong Q, Choy KL. Disturbing stability of interface by adopting phase-change temperature gradient to reduce ice adhesion strength. Cold Reg Sci Technol 2019;158:69–75. https://doi.org/10.1016/j.coldregions.2018.11.010.
[88] Fillion RM, Riahi AR, Edrisy A. Design factors for reducing ice adhesion. J Adhes Sci Technol 2017;31:2271–84. https://doi.org/10.1080/01694243.2017.1297588.
[89] Jo HH, Kim J, Kim S. Enhancing the power generation performance of photovoltaic system: impact of environmental and system factors. Appl Therm Eng 2024;240:122221. https://doi.org/10.1016/j.applthermaleng.2023.122221. ID.
[90] Lopez-Pascual D, Valiente-Blanco I, Fernandez-Munoz M, Diez-Jimenez E. Theoretical modelling and optimization of a geothermal cooling system for solar photovoltaics. Renew Energy 2023;206:357–66. https://doi.org/10.1016/j.renene.2023.01.098.